Semiconductor Physics, Quantum Electronics & Optoelectronics, 2009. V. 12, N 1. P. 35-41.

PACS 61.72.Dd, 68.55.-a, 78.20.Ci, 78.67.-n

The substructural and optical characteristics of ZnTe thin films

M.M. Kolesnyk[1], D.I. Kurbatov[1], A.S. Opanasyuk[1], V.B. Loboda[2]
[1]*Sumy State University, 2, Rymsky-Korsakov str., 40007 Sumy, Ukraine*
[2]*Sumy State Pedagogical University, 87, Romenska str., 40002 Sumy, Ukraine*
E-mail: maxxkol@yahoo.com; kurd@ukr.net; opanasyuk_sumdu@ukr.net

Abstract. The substructural and optical characteristics of ZnTe thin films obtained by close-spaced vacuum sublimation technique under different condensation conditions were investigated. The size of coherent scattering regions (CSR), the level of microstrain, stacking fault defects concentration in condensate, the average dislocations density on the subgrain boundaries and their volume were estimated with X-ray diffraction line broadening using the Hall method and the method of threefold convolution. It is shown that the mechanism of CSR size increase and the microdeformation level reduction are of the activation nature. Spectral distributions of transmission coefficient $T(\lambda)$, refractive index $n(\lambda)$, extinction coefficient $k(\lambda)$ and their dependences on the deposition temperature of ZnTe films are obtained.

Keywords: ZnTe thin film, X-ray analysis, coherent scattering region, microstrain, refractive index, extinction coefficient, optical band gap.

Manuscript received 12.09.08; accepted for publication 18.12.08; published online 30.01.09.

1. Introduction

Recently there has been observed a growing interest to ZnTe thin films studying. This attention is related to possibility of creating the number of high-performance electronic devices on the basis of these thin layers [1]. ZnTe films are used as a back contact for *p*-CdTe layers in solar cells with CdS/CdTe heterojunction [2]. ZnTe is perspective material for designing the emission diodes and lasers operating in the green spectral region, photodetectors, and devices operating under THz frequencies [3]. The fact that this semiconductor does not contain cadmium is an important condition from the ecological point of view.

The basic requirements for thin films are as follows: chemical composition should be close to the stoichiometric one, single-phase and textured columnar structure with low concentration of stacking fault defects (SFD) and growth twins. However, plenty of researches concerning II-VI thin films indicate specific properties, namely: co-existence of two polymorphic phases, zinc-blende (ZB) and wurtzite (WZ), lamellar structure of the crystallite, high concentration of SFD and growth twins, high level of microstresses and macrostresses, a tendency to anomalous axial texture formation, etc., prevention or removal of which is a complex technological problem [4]. This structural peculiarities of chalcogenide thin films, finally, determine the electro-physical and optical properties of layers.

Electrodeposition [5-6], high-frequency cathode sputtering [2, 7], pulse laser deposition [8] and thermal evaporation [1, 9], close-spaced vacuum sublimation (CSVS) [10] are only some technologies used for obtaining ZnTe thin films. The latter method has proved its effectiveness when covered by different multicomponent semiconductors [11]. Therefore, CSVS method is widely used for the deposition of the II-VI compound thin films [12-14]. At the same time, microstructural and optical characteristics obtained by CSVS technique, as well as their dependence on physical-and-technological conditions of the thin film growth have not been studied thoroughly.

2. Experimental details

ZnTe thin films were deposited on cleaned glass substrates by CSVS method. The powder of the stoihiometric compounds was used as a source material. Charge of ZnTe have ZB structure with its lattice parameter $a = 0.60990$ nm. During deposition of the thin films, the evaporator temperature was $T_e = 973$ K. A substrate temperature was changed within the range $T_s = 323$-773 K.

Structural investigations of the films were performed using X-ray diffractometer DRON 4-07 with

Ni-filtered K_αCu radiation source and conventional Bragg-Brentano geometry. Continuous mode scanning over the range of diffraction angles $20° \le 2\theta \le 80°$ (where 2θ is the Bragg angle) was applied to examine the surface of the samples. Obtained diffraction patterns were normalized to the intensity of (111) peak.

XRD method was also applied to determine the sizes (L) of the coherent scattering regions (CSR) and microdeformation level ($\varepsilon = \Delta d/d$) in the thin films with account for broadening of diffraction peaks. To distinguish the diffraction broadening caused by physical and instrumental effects, the approximations of line profile by Cauchy and Gaussian were used. Calculations were carried out according to the Hall method [15-16]. Besides, microdeformation levels and sizes of CSR were immediately determined from the threefold convolution describing XRD line's broadening by the method [17].

Optical properties of the films were investigated by double-beam spectrophotometer SF-46 within the range of wavelengths λ = 520-760 nm under room temperature. Spectra of optical transmission $T(\lambda)$ and optical density $D(\lambda)$ of ZnTe were measured, too. Further, spectral distributions of the absorption coefficient $\alpha(\lambda)$ were calculated from the $T(\lambda)$ spectra wiyhin the range of strong light absorption by using the Lambert expression $\alpha = -\ln(T)/l$, where l – thickness of the films [18].

3. Results and discussion

The peculiarities of ZnTe thin films growth process and some of their structural characteristics were the object of our research earlier [19]. At low substrate temperatures, low increase of the crystallite size was observed, and the crystallite shape of crystallite was close to equiaxial. At high substrate temperatures, the mechanism of growth changed, and thin films had a columnar structure. The diameter of the columnar-like grains d depends on growth conditions and the film thickness l. Under increase of T_s their average size in the film plane rises.

Our analysis of XRD patterns has demonstrated that ZnTe layers have ZB structure (Fig. 1), WZ phase is not observed. The (111) and (222) peaks with dominant maximum intensities are present in most of the cases and exhibit the strong texture of the films. Calculations by the reciprocal pole figures method allowed to determine axial growth texture [111] in chalcogenide thin films perfection of which is increased with the layer thickness and depends on growth conditions.

It is known that physical broadening of diffraction lines is caused by dispersity of CSR, lattice microstrains and concentration of SFD [11-12]. The analysis of diffraction profiles with determination of the mentioned causes is well established in the investigations of polycrystalline materials [15-16], but to examine chalcogenide it is rarely used. Usually, diffraction line broadening is ascribed to CSR dispersity only, which can be determined by the well-known Debye-Scherrer formula [7, 14].

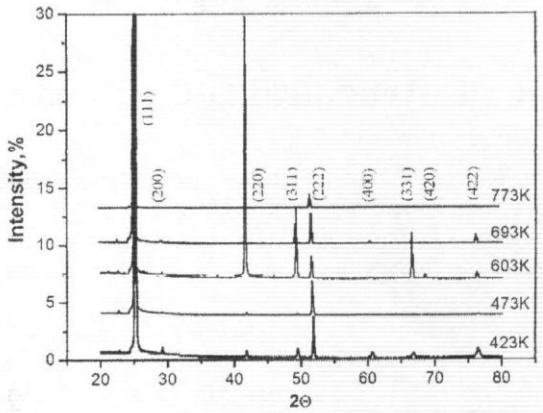

Fig. 1. XRD patterns of ZnTe thin films obtained under different substrate temperatures T_s.

The pairs of lines, (111) and (222) or (200) and (400), were chosen for estimation of microstructural parameters of ZnTe. Fig. 2 presents the typical Hall graphs. As it is shown, the points obtained by reflexes from (hhh) and (h00) planes are found at different lines having in most of the cases different slopes relatively to the x axis.

It is known that interception of the corresponding line with the y axis gives CSR size (L) in the direction normal to the planes set, and the slope of this line points out a microdeformation level (ε) in the films. Table 1 presets corresponding data obtained from Cauchy and Gaussian approximations. Values of the microstructural characteristics calculated by these approximations are in good correlation. But these approximations allow determining only the most and least CSR size value L and microdefects ε in thin films. Thus, the experimental error can reach 30-50 % [15-17].

The method of threefold convolution applied for XRD patterns gives more precise data of CSR values and microdeformation compared to those obtained by the classical Hall method. The parameters of the film substructure can be found from the expressions [17]

$$L = \frac{\lambda}{\cos\theta_1} \cdot \frac{tB_1 - cB_2}{t\beta_1^2 - \beta_2^2}, \qquad (1)$$

$$\varepsilon^2 = \frac{c\beta_1^2 B_2 - \beta_2^2 B_1}{16\,\mathrm{tg}\theta_1 \left(c\,B_2 - t\,B_1\right)}, \qquad (2)$$

where λ is the X-ray radiation wavelength; $t = \dfrac{\mathrm{tg}^2\theta_2}{\mathrm{tg}^2\theta_1}$; $c = \dfrac{\cos\theta_1}{\cos\theta_2}$; $\beta_i = \sqrt{(B_1)^2 - (b_i)^2}$; θ_1 and θ_2 are diffraction angles of the pair of lines under analysis; B, b, β are measured, instrumental and physical broadening of the corresponding X-ray lines, respectively.

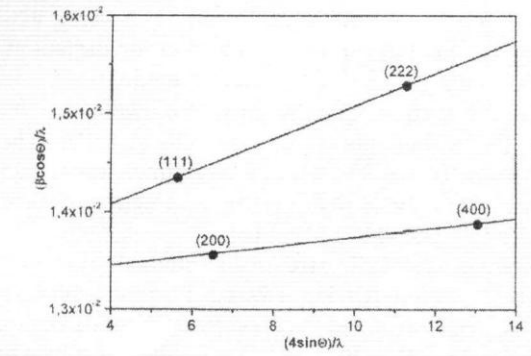

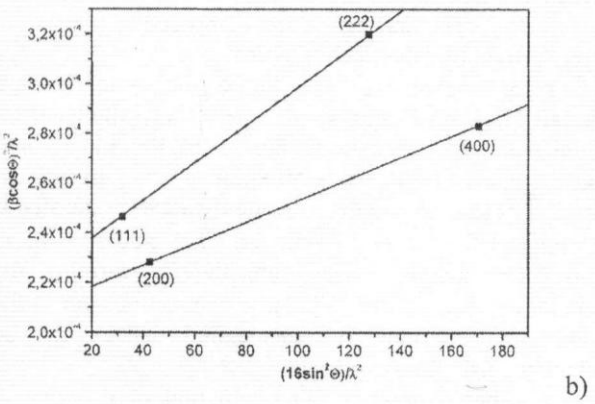

Fig. 2. Hall graphs plotted at X-ray diffraction of ZnTe thin film, obtained at $T_s = 693$ K. Cauchy approximations (a) and Gaussian approximations (b).

The results of the calculations for L and ε by the method of threefold convolution for ZnTe are presented in Table 1. The latter data of L and ε values obtained from the expressions (1) and (2) are found in most cases intervening between Gaussian and Cauchy approximations. It indicates the reliability of the results obtained from the analysis of X-ray line broadening. Thus, in accordance with [17] dimensional accuracy of CSR and level of microdeformation in condensates by the method of threefold convolution are not worse than 11-16 % depending on conditions of X-ray pattern reading.

As parameter points of substructure of ZnTe films particular from threefold convolution are the most precise and close to the real ones, the further discussion of results and calculations were carried out by us after them.

CSR size in the direction perpendicular to planes (111) in ZnTe films at first grows (from $L = 59$ nm to $L = 69$ nm) as the substrate temperature T_s increases and then reveales some lowering ($L = 62$ nm) with further increase of T_s (Table 1). As it is seen, there is an optimal temperature interval ($T_s = 600$-700 K), at which the CSR in thin films is maximal. The lattice microstrains in ZnTe films decrease from $1.3 \cdot 10^{-3}$ to $0.6 \cdot 10^{-3}$ as T_s is raised (Table 1).

CSR size behaves differently in the direction perpendicular to crystallographic planes (200), it reduces with the substrate temperature growth from $L \sim 94$ nm to ~ 69 nm, becoming close to the CSR size in the direction perpendicular to planes (111). Simultaneously, the level of microdeformations slightly rises from $\varepsilon \sim 0.3 \cdot 10^{-3}$ to $\sim 0.5 \cdot 10^{-3}$, again approaching the value ε in another direction. It should be mentioned that, as a result of the low (200) and (400) peak intensities measuring their subbroadening was performed with a considerable error, so the data of L and ε are less reliable.

In Fig. 3 you can see the data for the substructure of ZnTe films, determined using threefold convolution, are given in the coordinates $\ln L - 10^3 / T_s$

Table 1. The characteristic of ZnTe thin film substructure.

T_s, K	(*hkl*)	L, nm			ε, 10^3			α′, %
		Approximation		Convo-	Approximation		Convo-	
		Gaussian	Cauchy	lution	Gaussian	Cauchy	lution	
powder	(111)-(222)	28.57	36.45	37.54	2.03	2.05	1.19	1.43
	(200)-(400)	96.24	72.21	75.21	0.67	1.33	1.07	
323	(111)-(222)	46.58	57.99	59.39	0.87	1.60	1.29	0.67
	(200)-(400)	90.48	94.18	94.25	0.35	0.40	0.33	
423	(111)-(222)	64.81	63.92	63.93	0.70	1.37	1.11	0.53
	(200)-(400)	47.47	48.64	48.65	0.37	0.54	0.42	
468	(111)-(222)	69.35	65.43	65.54	0.15	0.63	0.43	0.12
	(200)-(400)	91.19	62.98	70.65	0.78	1.46	0.79	
473	(111)-(222)	54.23	60.41	60.76	0.72	0.93	0.64	–
	(200)-(400)	–	–	–	–	–	–	
603	(111)-(222)	65.36	68.78	68.87	0.45	0.62	0.46	0.15
	(200)-(400)	65.72	75.29	75.98	0.67	0.73	0.51	
693	(111)-(222)	74.54	67.13	67.50	0.17	0.88	0.64	0.04
	(200)-(400)	75.55	69.07	69.34	0.049	0.66	0.46	
773	(111)-(222)	59.05	61.99	62.07	0.46	0.66	0.49	–
	(200)-(400)	–	–	–	–	–	–	

($\ln\sigma - 10^3/T_s$). As it is seen from the figure, the processes determining the dispersity degree of substructure elements and the microdeformation level in the films belong to the thermally activated ones [3].

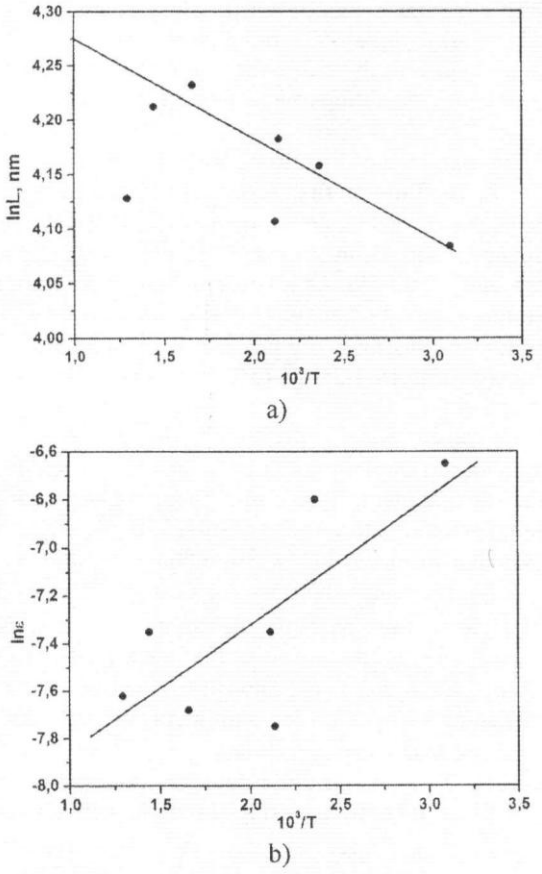

Fig. 3. The influence of T_s on the CSR size (a) and level of microdeformations (b) in ZnTe thin films.

The microstress level in ZnTe films was calculated according to the known values of microdeformations (Table 2) with using the Yung modulus value $E = 64$ GPa. It is found that the microstress values in the samples lie within the range $\sigma =$ 20-83 MPa. The maximal value of $\sigma = 83$ MPa is 3 to 5 times lower than that investigated by X-ray method in electrodeposited films ZnTe ($\sigma =$ 262-4429 MPa) [6].

Moreover, the CSR size in the studied films was close to that found in [6], but it was 2-3 times larger than in the layers obtained by vacuum condensation technology in [9, 20, 21]. So, the results of investigations concerning the ZnTe film substructure show better structural perfection compared to that of the layers grown by other technologies.

It is known that the block subboundaries are formed by dislocations set on their boundaries, simultaneously dislocations placed in the block bulk cause material microdeformations. It gives the possibility to evaluate the average dislocation density at the microdeformation size ε and CSR size L in these films. The average dislocation density forming the boundaries is in accord to [22]. If dislocations are in the middle of subgrains, the dislocation density can be calculated using the expression [22].

Another expression for evaluation of the general dislocation concentration in the material is given in [6]

$$\rho = \frac{\sqrt{12}\,\varepsilon}{d\,L}. \qquad (3)$$

where d is the period of material lattice in a corresponding direction.

The calculation results of the average dislocation density in thin films by using the expressions (3) are given in Table 2. The data in terms of order correlate with each other. As it is seen, thin films are

Table 2. Dislocation density in ZnTe films.

T_s, K	(*hkl*)	L, nm	ε, 10^3	σ, MPa	ρ_L, 10^{-13}, lin/m^2	ρ_ε, 10^{-13}, lin/m^2	ρ, 10^{-13}, lin/m^2
powder	(111)-(222)	37.54	1.19	76.16	212.9	18.3	31.2
	(200)-(400)	75.21	1.07	68.48	53.0	19.7	16.2
323	(111)-(222)	59.39	1.29	82.56	85.1	21.5	21.4
	(200)-(400)	94.25	0.33	21.12	33.8	1.9	3.98
423	(111)-(222)	63.93	1.11	71.04	73.4	15.9	17.1
	(200)-(400)	48.65	0.42	26.88	126.8	3.0	9.8
468	(111)-(222)	65.54	0.43	27.52	69.8	2.4	6.5
	(200)-(400)	70.65	0.79	50.56	60.1	10.7	12.7
473	(111)-(222)	60.76	0.64	40.96	81.3	5.3	10.4
	(200)-(400)	–	–	–	–	–	–
603	(111)-(222)	68.87	0.46	29.44	63.3	2.7	6.6
	(200)-(400)	75.98	0.51	32.64	51.9	4.5	7.6
693	(111)-(222)	67.50	0.64	40.96	65.8	5.3	9.3
	(200)-(400)	69.34	0.46	29.44	62.4	3.6	7.5
773	(111)-(222)	62.07	0.49	31.36	77.9	3.1	7.8

characterized by a low concentration of dislocations (see [6]) that in general focus on the CSR boundaries. The CSR bulk is practically free of dislocations, one dislocation occurs in 10 blocks, approximately.

Three different methods of CSR size calculation give $L_{(h00)} > L_{(hhh)}$. Two explanations seemed to be possible: 1) CSR are not equiaxial, with sizes in direction perpendicular to crystallographic planes (111) less than those in direction perpendicular to planes (200); 2) CSR are equiaxial, but SFD contribute to broadening of lines corresponding to reflexes from (*hhh*) planes.

Let's consider the first assumption in more detail. The metallographic investigations allow to ascertain that CSR are significantly lower than grain sizes. In our opinion, in the direction perpendicular to crystallographic planes (111) these sizes are restricted by twins, SFD, and CSR themselves have the shape close to the cylindrical one. At the same time, the cylinder height $L_{(hhh)}$ is less than its diameter.

Assuming that CSR are equiaxial and additional broadening (111) and (222) lines due to SFD appeare, one can calculate the concentrations of growth and deformational defects [22]:

$$\alpha' = 1.5\alpha + \beta' = 3.04\left(\frac{1}{L_{(h00)}} - \frac{1}{L_{(hhh)}}\right) d_{(111)}, \qquad (4)$$

where α' is the concentration of deformational SFD, β' is the concentration of growth SFD, $d_{(111)}$ is an interplanar spacing.

Table 1 presents the corresponding results. It is obvious that the total concentration of SFD decreases as T_s is raised from 0.67 % (T_s = 323 K) to 0.04 % (T_s = 693 K). The highest concentration of SFD was found in the charge (1.43 %).

These values are considerably lower than those found in the ZnTe electrodeposited thin films, obtained at temperatures T_s = 303-363 K (α' = 1.5-8.5 %) [6]. Like to the electrodeposited films [6], we can observe the tendency of SFD concentration to decrease with increasing the temperature of synthesis. The results obtained testify to more equal conditions of thin films condensation in the case of chalcogenide evaporation in CSVS. They correlate well with the data about thermodynamic parameters for sfalerit and wurtzite combined phases. With increasing T_n, the resistance of cubic ZnTe increases, the probability of breaking of plane sequence (111) decreases, the concentration of SFD decreases, correspondingly.

To determine the optical band gap (BG) E_g of ZnTe from transmission spectra $T(\lambda)$, we have applied the common expression valid for direct-gap and indirect-gap semiconductors:

$$\alpha h\nu = A\left(h\nu - E_g\right)^m, \qquad (5)$$

where A is a constant depending on the effective mass of the charge carriers in the material; $h\nu$ is the incident photon energy; α is the absorption coefficient; m is determined by the mechanism of photon absorption in semiconductors; for direct materials (ZnTe is a direct-gap compound) m = 1/2. Therefore, the extrapolation of linear part $(\alpha h\nu)^2 - h\nu$ -dependence down to interception with the energy axis enables to determine the BG of semiconductor (Fig. 4).

As seen from Fig. 4, the BG values of the layers obtained at different substrate temperatures vary smaller. As the substrate temperature increases from 393 to 773 K the gap changes from E_g = 2.22 eV to 2.23 eV, respectively. These results are somewhat lower than the data for single crystal ZnTe (E_g = 3.26 eV) and are in a good agreement with the data obtained for ZnTe layers by the method of thermal evaporation in vacuum (E_g = 2.0-2.2 eV) [20-21]. Recently, the effect of bandgap reduction in chalcogenides has been related with dissolving the additional isovalent impurity (oxygen) in them [23].

From the spectra of light transmission in the range of weak absorption, we have calculated reflection spectra $R(\lambda)$, spectral distributions of refractivity $n(\lambda)$, and extinction $k(\lambda)$ of ZnS films. These coefficients are bound by the Fresnel expression:

$$R = \frac{(n-1)^2 + k^2}{(n+1)^2 + k^2}, \qquad (6)$$

where $k = \frac{\alpha\lambda}{4\pi}$.

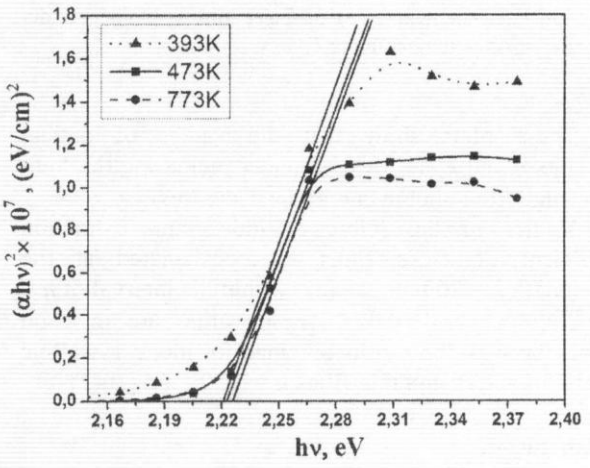

Fig. 4. $(\alpha h\nu)^2 - h\nu$ dependence of ZnTe films obtained at different substrate temperatures T_s.

Calculating k the refractive index of the material can be found:

$$n = \left(\frac{1+R}{1-R}\right) + \sqrt{\frac{4R}{(1-R)^2} - k^2}. \qquad (7)$$

The spectral distributions of these optical coefficients are plotted in Fig. 5.

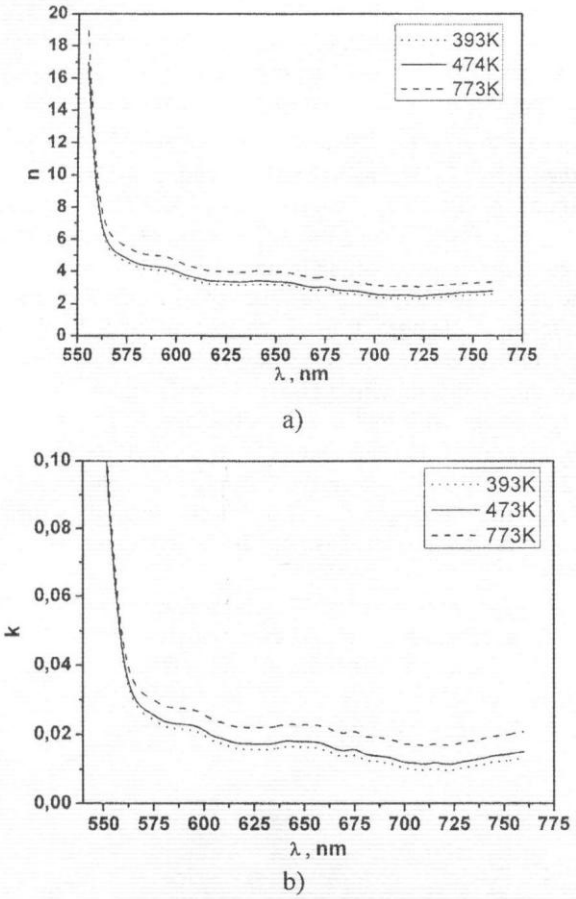

Fig. 5. Spectral distributions of the refractive index $n(\lambda)$ (a) and extinction coefficient $k(\lambda)$ (b) of ZnTe films obtained under different substrate temperatures T_s.

These plots show that the values of optical constants n and k are lowered under increasing the light wavelength (the photon energy $h\nu$ decreases).

Values of the refractive index and extinction coefficient of ZnTe films were calculated at the wavelength λ = 700 nm, and lie within the interval of n = 2.59-2.69 (k = 0.01-0.02). These values are in good correlation with the results obtained for monocrystalline material n = 2.70 and thin films n = 2.50-2.65 [20-21].

4. Conclusion

The substructural and optical characteristics of ZnTe thin films obtained by close-spaced vacuum sublimation technique under different condensation conditions were investigated. The size of CSR, the level of microstrains, fault defect concentration in condensate, the average dislocations density on the subgrain boundaries and in their bulk were estimated with X-ray diffraction line broadening using the Hall method and the method of threefold convolution. It is shown, at first the CSR grows (from L = 59 nm to 69 nm) as the substrate temperature T_s increased and then revealed some lowering (L = 62 nm) with further increasing of T_s. There is the optimal temperature interval (T_s = 600-700 K), at which the CSR in thin films is maximal. The lattice microstrain in ZnTe films from $1.3 \cdot 10^{-3}$ to $0.6 \cdot 10^{-3}$ decreases with T_s. It is obvious that the total concentration of SFD decreases when T_s is raised from 0.67 % (T_s = 323 K) to 0.04 % (T_s = 693 K). It is shown that the mechanisms of CSR size increase and the microdeformation level reduction are of the activation nature.

Spectral distributions of the transmission coefficient $T(\lambda)$, refractive index $n(\lambda)$, extinction coefficient $k(\lambda)$ and their dependence on the deposition temperature of ZnTe films are obtained. Values of the refractive index and extinction coefficient of ZnTe films were calculated at the wavelength λ = 700 nm, and lie in the interval of n = 2.59-2.69 (k = 0.01-0.02).

These results testify about equal conditions of film condensation under chalcogenide evaporation in CSVS and perspectives of applying the method to obtain condensates with high structural perfection, suitable for usage in various electronic devices.

Acknowledgments

The authors would like to thank Ph.D. S. Danilchenko from Applied Physical Institute (Sumy) for XRD investigations of thin films ZnTe

References

1. E.E. Khawaja, M.A. Al-Daous, S.M.A. Durrani et al., Chemical inhomogeneity in zinc telluride thin films prepared by thermal evaporation // *Thin Solid Films* **485**, p. 16-21 (2005).
2. T.A. Gessert, A.R. Mason, R.C. Reedy et al., Development of rf sputtered, Cu-doped ZnTe for use as a contact interface layer to p-CdTe // *J. Electr. Mater.* **24** (10), p. 1443-1449 (1995).
3. R. Bhargava, *Properties of Wide Band Gap II–VI Semiconductors.* The Institution of Electrical Engineers, London, United Kingdom, 1997.
4. P.A. Panchekha, Structure and technology problems of A_2B_6 semiconductor films // *Functional Materials* 7(2), p. 1-5 (2000).
5. A.E. Rakhshani, B. Pradeep, Thin films of ZnTe electrodeposited on stainless steel // *Appl.Phys.* **79**, p. 2021-2025 (2004).
6. T. Mahalingam, V.S. John, G. Ravi, P.J. Sebastian, Microstructural characterization of electro-synthesized ZnTe thin films // *Cryst. Res. Technol.* **37**(4), p. 329-339 (2002).
7. H. Bellakhder, A. Outzourhit, E.L. Ameziane, Stady of ZnTe thin films deposited by r.f. sputtering // *Thin Solid Films* **382**, p. 30-33 (2001).
8. A. Erlacher, A.R. Lukaszew et al., Structural and surface analysis of thin-film ZnTe formed with pulsed-laser deposition // *Surf. Sci.* **600,** p. 3762-3765 (2006).

9. A.A. Ibrahim, N.Z. El-Sayed, M.A. Kaid et al., Structural and electrical properties of evaporated ZnTe thin films // *Vacuum* **75,** p. 189-194 (2004).
10. J. Takahashi, K. Mochizuki, K. Hitomi et al., Growth of $Cd_{1-x}Zn_xTe$ film by hot-wall method and its evaluation // *J. Crys. Growth* **269**, p. 419-424 (2004).
11. A. Lopez-Otero, Hot wall epitaxy. Invited Review // *Thin Solid Films* **49**, p. 3-57 (1978).
12. I.P. Kalinkin, V.B. Alescovskiy, A.V. Simashkevich, *A_2B_6 Epitaxial Thin Films*. Leningrad State University, Leningrad, 1978 (in Russian).
13. Y.P. Venkata Subbaiah, P. Prathap, K.T. Ramakrishna Reddy, Structural, electrical and optical properties of ZnS films deposited by close-spaced evaporation // *Appl. Surf. Sci.* **253**, p. 2409-2415 (2006).
14. P. Prathap, Y.P. Venkata Subbaiah, K.T. Ramakrishna Reddy, R.W. Miles, Influence of growth rate on microstructure and optoelectronic behaviour of ZnS film // *J. Phys. D: Appl. Phys.* **40**, p. 5275-5282 (2007).
15. Y.S. Umanskiy, U.A. Skakov, A.N. Ivanov, *Crystallography, X-ray Diffraction and Electron Microscopy*. Publ. Metallurgiya, Moscow, 1982 (in Russian).
16. B.E. Warren, *X-ray Diffraction*. Dover, New York, 1990.
17. A.S. Kagan, L.M. Shishlyannikova, A.P. Unicel, Application the three-fold convolution approximation method of profiles X-ray diffraction lines // *Zavodskaya laboratoriya* **46** (10), p. 903-906 (1980) (in Russian).
18. J. Pankov, *Optical Processes in Semiconductors*. Mir, Moscow, 1973 (in Russian).
19. S. Danilchenko, T. Kalinichenko, M. Kolesnik et al., Structural characteristics of ZnTe thin films obtained by close-spaced vacuum sublimation technique // *Visnyk Sumskogo Derzhavnogo Universytetu* **1**, p. 117-123 (2007) (in Ukrainian).
20. R. Amutha, A. Subbarayan R. Sathyamoorthy, Influence of substrate temperature on microcrystalline structure and optical properties of ZnTe thin films // *Cryst Res. Technol.* **41** (12) p. 1174-1179 (2006).
21. L. Feng, D. Mao, J. Tang, R.T. Collins, J.U. Thefny, The structural, optical and electrical properties of vacuum evaporated Cu-doped ZnTe polycrystalline thin films // *J. Electr. Mater.* **25** (9), p. 1422-1427 (1996).
22. L.S. Palatnik, M.Ja Fuks, V.M. Kosevich, *Creation Mechanism and Substructure of Condensed Thin Films*. Nauka, Moscow, 1972 (in Russian).
23. N.K. Morosova, I.A. Karetnikov, K.V. Golub, N.D. Danilevich, V.M. Lisitzyn, V.I. Oleshko, The action of oxygen on ZnS electronic band structure // *Fizika tekhnika poluprovodnikov* **39** (5), p. 513-520 (2005) (in Russian).